
Generative Adversarial Examples

Yang Song

Stanford University

yangsong@cs.stanford.edu

Rui Shu

Stanford University

ruishu@cs.stanford.edu

Nate Kushman

Microsoft Research

nkushman@microsoft.com

Stefano Ermon

Stanford University

ermon@cs.stanford.edu

Abstract

Adversarial examples are typically constructed by perturbing an existing data point, and current defense methods are focused on guarding against this type of attack. In this paper, we propose a new class of adversarial examples that are synthesized entirely from scratch using a conditional generative model. We first train an Auxiliary Classifier Generative Adversarial Network (AC-GAN) to model the class-conditional distribution over inputs. Then, conditioned on a desired class, we search over the AC-GAN latent space to find images that are likely under the generative model and are misclassified by a target classifier. We demonstrate through human evaluation that this new kind of adversarial inputs, which we call *Generative Adversarial Examples*, are legitimate and belong to the desired class. Our empirical results on the MNIST, SVHN, and CelebA datasets show that generative adversarial examples can easily bypass strong adversarial training and certified defense methods which can foil existing adversarial attacks.

1 Introduction

Machine learning algorithms are known to be susceptible to adversarial examples. Samples from the dataset can be perturbed to mislead cutting edge classifiers [1, 2]. This has raised concern for safety-critical AI applications because attackers could use them to, for example, mislead autonomous driving vehicles [3, 4, 5] or hijack voice controlled intelligent agents [6, 7, 8].

To mitigate the threat of adversarial examples, a large number of methods have been developed. These include augmenting training data with adversarial examples [2, 9, 10, 11], removing adversarial perturbations [12, 13, 14], and encouraging a small Lipschitz constant for the classifier [15]. Recently, [16, 17] proposed theoretically-certified defenses based on minimizing convex upper bounds of the training loss under worst-case perturbations. Although inspired by different perspectives, a shared design principle of current defense methods is to make classifiers more robust to small perturbations.

In this paper, we consider a more general case, where adversarial examples are generated entirely from scratch instead of perturbing a given data point. In practice, an attacker might want to change an input significantly while not changing the semantics. Taking traffic signs as an example, an adversary performing perturbation-based attacks can draw graffiti [4] or place stickers [18] on an existing stop sign in order to exploit a classifier. The attacker might also replace the original stop sign with a new one that was specifically manufactured to be adversarial. In the latter case, the new stop sign does not have to be a close replica of the original one—the font could be different, the size could be smaller—as long as it is still identified as a stop sign by humans. We argue that *all inputs that fool the classifier without confusing humans can pose potential security threats*. In particular, we show that previous defense methods, including the certified ones [16, 17], are not effective against this more

general attack. Ultimately, we hope that identifying and solving such new vulnerabilities can shed light on the weaknesses of existing classifiers, and enable progress towards human-like methods.

Generating this new kind of adversarial examples, however, is challenging. It is clear that adding small noise is a valid mechanism for generating new images from a desired class—the label should not change if the perturbation is small enough. How can we generate completely new images from a given class? In this paper, we leverage recent advances in generative modeling [19, 20, 21]. Specifically, we train an Auxiliary Classifier Generative Adversarial Network (AC-GAN [20]) to model the set of legitimate images for each class. Conditioned on a desired class, we can search over the latent code of the generative model to find examples that are mis-classified by the model under attack, even when protected by the most robust defense methods available. The images that successfully fool the classifier without confusing humans (verified via Amazon Mechanical Turk [22]) are referred to as *Generative Adversarial Examples*. The efficacy of our attacking method is demonstrated on the MNIST [23], SVHN [24], and CelebA [25] datasets, where our attacks uniformly achieve over 84% success rates. In addition, our generative adversarial examples show moderate transferability to other architectures, reducing the accuracy of a black-box certified classifier [17] by 35.2%.

2 Background

We review some recent work on adversarial examples, defense methods, and conditional generative models. Although adversarial examples can be crafted for many domains, we focus on image classification tasks in the rest of this paper, and will use the words “examples” and “images” interchangeably.

Adversarial examples Let $x \in \mathbb{R}^m$ denote an input image to a classifier $f : \mathbb{R}^m \rightarrow \{1, 2, \dots, k\}$, and assume the attacker has full knowledge of f (a.k.a., white-box setting). [1] discovered that it is possible to find a slightly different image $x' \in \mathbb{R}^m$ such that $\|x' - x\| \leq \epsilon$ but $f(x') \neq f(x)$, by solving a surrogate optimization problem with L-BFGS [26]. Different matrix norms $\|\cdot\|$ have been used, such as l_∞ ([9]), l_2 ([27]) or l_0 ([28]). Similar optimization-based methods are also proposed in [29, 30]. In [2], the authors observe that $f(x)$ is approximately linear and propose the Fast Gradient Sign Method (FGSM), which applies a first-order approximation of $f(x)$ to speed up the generation of adversarial examples. This procedure can be repeated several times to give a stronger attack named Projected Gradient Descent (PGD [10]).

Defense methods The current mainstay of defense methods is to make classifiers more robust to small perturbations of the image. There has been an “arms race” between increasingly sophisticated attack and defense methods. As indicated in [31], the strongest defenses to date are adversarial training [10] and certified defenses [16, 17]. In this paper, we focus our investigation of generative adversarial attacks on these defenses.

Generative adversarial networks (GANs) GAN [19] is composed of a generator $g_\theta(z)$ and a discriminator $d_\phi(x)$. The generator maps a source of noise $z \sim P_z$ to a synthetic image $x = g_\theta(z)$. The discriminator receives an image x and produces a value $d_\phi(x)$ to distinguish whether it is sampled from the true image distribution P_x or generated by $g_\theta(z)$. The goal of GAN training is to learn a discriminator to reliably distinguish between fake and real images, and a good generator to fool the discriminator. To stabilize training, we use the Wasserstein GAN [32] formulation with gradient penalty [21], which solves the following optimization problem

$$\min_{\theta} \max_{\phi} \mathbb{E}_{z \sim P_z} [d_\phi(g_\theta(z))] - \mathbb{E}_{x \sim P_x} [d_\phi(x)] + \lambda \mathbb{E}_{\tilde{x} \sim P_{\tilde{x}}} [(\|\nabla_{\tilde{x}} d_\phi(\tilde{x})\|_2 - 1)^2],$$

where $P_{\tilde{x}}$ is the distribution obtained by sampling uniformly along straight lines between pairs of samples from P_x and generated images from $g_\theta(z)$, $z \sim P_z$.

To generate adversarial examples with the intended semantic information, we also need to control the labels of the generated images. One popular method of incorporating label information into the generator is Auxiliary Classifier GAN (AC-GAN [20]), where the conditional generator $g_\theta(z, y)$ takes label y as input and an auxiliary classifier $c_\psi(x)$ is introduced to classify both generative and real images. The optimization objectives are

$$\begin{aligned} & \min_{\theta} -\mathbb{E}_{z \sim P_z, y \sim P_y} [d_\phi(g_\theta(z, y)) - \log p(c_\psi(g_\theta(z, y)) = y)] \\ & \min_{\phi, \psi} \mathbb{E}_{z \sim P_z, y \sim P_y} [d_\phi(g_\theta(z, y))] - \mathbb{E}_{x \sim P_x} [d_\phi(x)] - \mathbb{E}_{x \sim P_x, y \sim P_{y|x}} [\log p(c_\psi(x) = y)] \\ & \quad + \lambda \mathbb{E}_{\tilde{x} \sim P_{\tilde{x}}} [(\|\nabla_{\tilde{x}} d_\phi(\tilde{x})\|_2 - 1)^2], \end{aligned}$$

where $p(\cdot)$ denotes the probability, $d_\phi(\cdot)$ is the discriminator, P_y represents a uniform distribution over all labels $\{1, 2, \dots, k\}$, $P_{y|x}$ denotes the ground-truth distribution of y given x , and P_z is chosen to be $\mathcal{N}(0, 1)$ in our experiments.

3 Methods

3.1 Generative adversarial examples

We start this section by formally characterizing perturbation-based and generative adversarial examples. Let \mathcal{I} be the set of all digital images under consideration. Suppose $o : \mathcal{O} \subseteq \mathcal{I} \rightarrow \{1, 2, \dots, K\}$ is an oracle that takes an image in its domain \mathcal{O} and outputs one of K labels. In addition, we consider a classifier $f : \mathcal{I} \rightarrow \{1, 2, \dots, K\}$ that can give a prediction for any image in \mathcal{I} , and assume $f \neq o$. Equipped with those notations, we can provide definitions used in this paper:

Definition 1 (Perturbation-Based Adversarial Examples). *Given a subset of (test) images $\mathcal{T} \subset \mathcal{O}$, small constant $\epsilon > 0$, and matrix norm $\|\cdot\|$, a perturbation-based adversarial example is defined to be any image in $\mathcal{A}_p \triangleq \{x \in \mathcal{O} \mid \exists x' \in \mathcal{T}, \|x - x'\| \leq \epsilon \wedge f(x') = o(x') = o(x) \neq f(x)\}$.*

In other words, traditional adversarial examples are based on perturbing a correctly classified image in \mathcal{T} so that f gives an incorrect prediction, according to the oracle o .

Definition 2 (Generative Adversarial Examples). *A generative adversarial example is any image that is an element of $\mathcal{A}_g \triangleq \{x \in \mathcal{O} \mid o(x) \neq f(x)\}$.*

In most previous work on perturbation-based adversarial examples, the oracle o is implicitly defined as a black box that gives ground-truth predictions of human beings, \mathcal{T} is chosen to be the test dataset, and $\|\cdot\|$ is usually one of l_∞ ([9]), l_2 ([27]) or l_0 ([28]) matrix norms. Since o corresponds to human beings, \mathcal{O} should represent all images that look realistic to humans, including those with small perturbations. From the definition it is clear that $\mathcal{A}_p \subset \mathcal{A}_g$, which means our proposed generative adversarial examples is a strict generalization of traditional perturbation-based adversarial examples.

3.2 Practical generative adversarial attacks

The key to practically producing generative adversarial examples is to model the set of legitimate images \mathcal{O} . We do so by training a generative model $g(z, y)$ —hence the name *Generative Adversarial Examples*—to map a random variable $z \in \mathbb{R}^m$ and a label $y \in \{1, 2, \dots, K\}$ to a legitimate image $x = g(z, y) \in \mathcal{O}$ satisfying $o(x) = y$. If the generative model is ideal, we will have $\mathcal{O} \equiv \{g(z, y) \mid y \in \{1, 2, \dots, K\}, z \in \mathbb{R}^m\}$. Given such a model we can in principle enumerate all generative adversarial examples for a given classifier f , by finding all z and y such that $f(g(z, y)) \neq y$.

In practice, we can exploit different approximations of the ideal generative model to produce different kinds of generative adversarial examples. Because of its reliable conditioning and high fidelity image generation, we choose AC-GAN [20] as our basic class-conditional generative model. In what follows, we explore two attacks derived from variants of AC-GAN (see pseudocode in Appendix B).

Basic attack Let $g_\theta(z, y)$, $c_\phi(x)$ be the generator and auxiliary classifier of AC-GAN, and let $f(x)$ denote the classifier that we wish to attack. We focus on *targeted* generative adversarial attacks, where the attacker tries to generate an image x so that $o(x) = y_{\text{source}}$ but $f(x) = y_{\text{target}}$. In order to produce generative adversarial examples, we propose to find the appropriate z by minimizing a loss function \mathcal{L} that is carefully designed to produce high quality generative adversarial examples.

We decompose the loss as $\mathcal{L} = \mathcal{L}_0 + \lambda_1 \mathcal{L}_1 + \lambda_2 \mathcal{L}_2$, where λ_1, λ_2 are positive hyperparameters for weighting different terms. The first component

$$\mathcal{L}_0 \triangleq -\log p(f(g_\theta(z, y_{\text{source}}))) = y_{\text{target}} \quad (1)$$

encourages f to predict y_{target} , where $p(\cdot)$ denotes probability. The second component

$$\mathcal{L}_1 \triangleq \frac{1}{m} \sum_{i=1}^m \max\{|z_i - z_i^0|, \epsilon\} \quad (2)$$

soft-constrains the search region of z so that it is close to a randomly sampled noise vector z^0 . Here $z = (z_1, z_2, \dots, z_m)$, $\{z_1^0, z_2^0, \dots, z_m^0\} \stackrel{\text{i.i.d.}}{\sim} \mathcal{N}(0, 1)$, and ϵ is a small positive constant. For a good generative model, we expect that $x^0 = g_\theta(z^0, y_{\text{source}})$ is diverse for randomly sampled z^0 and $o(x^0) = y_{\text{source}}$ holds with high probability. Therefore, by reducing the distance between z and z^0 , \mathcal{L}_1 has the effect of generating more diverse adversarial examples from class y_{source} . Finally

$$\mathcal{L}_2 \triangleq -\log p(c_\phi(g_\theta(z, y_{\text{source}})) = y_{\text{source}}) \quad (3)$$

encourages the auxiliary classifier c_ϕ to give correct predictions. We hypothesize that c_ϕ is relatively uncorrelated with f , which can possibly promote the generated images to reside in class y_{source} .

Note that \mathcal{L} can be easily modified to perform *untargeted* attacks, for example replacing \mathcal{L}_0 with $-\max_{y \neq y_{\text{source}}} \log p(f(g_\theta(z, y_{\text{source}})) = y)$. Different from perturbing an existing image, where it is reasonable to assume the true label does not change if the perturbation is small, we need human validation of our generative adversarial examples because they are created from scratch. To test whether the images are legitimate and belong to class y_{source} , we use crowd-sourcing on Amazon Mechanical Turk (MTurk).

Noise-augmented attack The expressive power of the AC-GAN generator can be improved if we add small trainable noise to the generated image. Let ϵ_{attack} be the maximum magnitude of noise that we want to apply. The noise-augmented generator is defined as $g_\theta(z, \tau, y; \epsilon_{\text{attack}}) \triangleq g_\theta(z, y) + \epsilon_{\text{attack}} \tanh(\tau)$, where τ is an auxiliary trainable variable with the same shape as $g_\theta(z, y)$ and \tanh is applied element-wise. As long as ϵ_{attack} is small, $g_\theta(z, \tau, y; \epsilon_{\text{attack}})$ should be indistinguishable from $g_\theta(z, y)$, and $o(g_\theta(z, \tau, y; \epsilon_{\text{attack}})) = o(g_\theta(z, y))$, i.e., adding small noise should preserve image quality and ground-truth labels. Similar to the basic attack, noise-augmented generative adversarial examples can be obtained by solving $\min_{z, \tau} \mathcal{L}$, with $g_\theta(z, y_{\text{source}})$ in (1) and (3) replaced by $g_\theta(z, \tau, y_{\text{source}}; \epsilon_{\text{attack}})$.

One interesting observation is that traditional perturbation-based adversarial examples can also be obtained as a special case of our noise-augmented attack, by choosing a suitable $g_\theta(z, y)$ instead of the AC-GAN generator. Specifically, let \mathcal{T} be the test dataset, and $\mathcal{T}_y = \{x \in \mathcal{T} \mid o(x) = y\}$. We can use a discrete latent code $z \in \{1, 2, \dots, |\mathcal{T}_{y_{\text{source}}}| \}$ and specify $g_\theta(z, y)$ to be the z -th image in \mathcal{T}_y . Then, when z^0 is uniformly drawn from $\{1, 2, \dots, |\mathcal{T}_{y_{\text{source}}}| \}$, $\lambda_1 \rightarrow \infty$ and $\lambda_2 = 0$, we will recover an objective similar to FGSM [2] or PGD [10].

4 Experiments

4.1 Experimental details

Amazon Mechanical Turk settings In order to demonstrate the success of our generative adversarial examples, we need to verify that their ground-truth labels disagree with the classifier’s predictions. To this end, we use Amazon Mechanical Turk (MTurk) to manually label each generative adversarial example.

To improve signal-to-noise ratio, we assign the same image to 5 different workers and use the result of a majority vote as ground-truth. For each worker, the MTurk interface contains 10 images and for each image, we use a button group to show all possible labels. The worker is asked to select the correct label for each image by clicking on the corresponding button. In addition, each button group contains an “N/A” button that the workers are instructed to click on if they think the image is not legitimate or does not belong to any class. To confirm our MTurk setup results in accurate labels, we ran a test to label MNIST images. The results show that **99.6%** of majority votes obtained from workers match the ground-truth labels.

For some of our experiments, we want to investigate whether generative adversarial examples are more similar to existing images in the dataset, compared to perturbation-based attacks. We use the classical A/B test for this, *i.e.*, each adversarial example is randomly paired with an existing image from the dataset, and the annotators are asked to highlight the synthesized images. Screen shots of all our MTurk interfaces can be found in Appendix E.

Datasets The datasets used in our experiments are MNIST [23], SVHN [24], and CelebA [25]. Both MNIST and SVHN are images of digits. For CelebA, we group the face images according to

Table 1: Attacking certified defenses on MNIST. The generative adversarial examples here are untargeted and without noise-augmentation. Numbers represent success rates (%) of our attack, based on human evaluations on MTurk. No perturbation-based attack with $\epsilon = 0.1$ can have a success rate larger than the *certified rate*, when evaluated on the training set.

Source Classifier	0	1	2	3	4	5	6	7	8	9	Certified Rate ($\epsilon = 0.1$)	Overall
Raghunathan et al. [16]	90.8	48.3	86.7	93.7	94.7	85.7	93.4	80.8	96.8	95.0	35.0	86.6
Kolter & Wang [17]	94.2	57.3	92.2	94.0	93.7	89.6	95.7	81.4	96.3	93.5	5.8	88.8

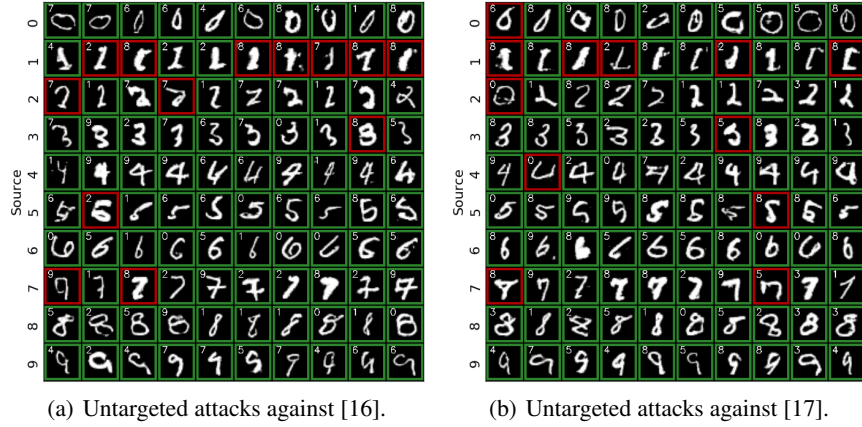


Figure 1: Random samples of untargeted generative adversarial examples (w/o noise) against certified defenses on MNIST. Green and red borders indicate success/failure respectively, according to MTurk results. The annotation in upper-left corner of each image represents the classifier’s prediction. For example, the entry in the top left corner (left panel) is classified as 0 by MTurk, and as a 7 by the classifier, and is therefore considered a success. The entry in the top left corner (right panel) is not classified as 0 by MTurk, and is therefore counted as failed.

female/male, and focus on gender classification. We test our attack on these datasets because the tasks (digit categorization and gender classification) are easier and less ambiguous for MTurk workers, compared to those having more complicated labels, such as Fashion-MNIST [33] or CIFAR-10 [34].

Model Settings We train our AC-GAN [20] with gradient penalty [21] on all available data partitions of each dataset, including training, test, and extra images (SVHN only). This is based on the assumption that attackers can access a large number of images. We use ResNet [35] blocks in our generative models, mainly following the architecture design of [21]. For training classifiers, we only use the training partition of each dataset. We copy the network architecture from [10] for the MNIST task, and use a similar ResNet architecture to [13] for other datasets. For more details about architectures, hyperparameters and adversarial training methods, please refer to Appendix C.

4.2 Untargeted attacks against certified defenses

We first show that our new adversarial attack can defeat the recently proposed *certified defenses* [16, 17]. These defenses can provide a theoretically verified certificate that a training example cannot be classified incorrectly by any perturbation-based attack with a perturbation size less than a given ϵ .

Setup For each source class, we use our method to produce 1000 untargeted generative adversarial examples without noise-augmentation. By design our method confirms that these are all incorrectly classified by the target classifier, and then we report, in Tab. 1, the fraction that human annotators label as belonging to the intended source class. We conduct these experiments on the MNIST dataset in order to ensure a fair comparison, since the classifier architectures along with weights for this dataset can be obtained directly from the authors of [16, 17]. We produce untargeted generative adversarial examples in this task, as the certificates are for untargeted attacks.



Figure 2: Comparing PGD attacks (top) and ours (bottom) for [16] on MNIST. Here we have overall success rate 86.6%. PGD has success rate 86.0% with $\epsilon = 0.31$.

Table 2: Overall success rates of our targeted generative attacks. Success rates of PGD are provided to show that the network is adversarially-trained to be robust. [†]Best public result.

Robust Classifier	Accuracy	Success Rate of PGD	Our Success Rate (w/o Noise)	Our Success Rate (w/ Noise)	ϵ_{attack}
Madry network [10] on MNIST	98.4	10.4 [†]	85.2	85.0	0.3
ResNet (adv-trained) on SVHN	96.3	59.9	84.2	91.6	0.03
ResNet (adv-trained) on CelebA	97.3	20.5	91.1	86.7	0.03

Results Tab. 1 shows the results. We can see that the stronger of the two certified defenses, [17], provides a certificate for 94.2% of the samples in the MNIST test set with $\epsilon = 0.1$ (out of 1). Our technique is not perturbation-based, and so 88.8% of our samples are able to defeat this defense.

4.2.1 Evading human detection

One natural question is, *why not simply use a larger ϵ instead?* With a large enough ϵ , certified defenses will give weaker certificates, and so existing perturbation-based attacks can also fool the certified defenses with high success rates. We can see the downside of this approach in Fig. 2; the resulting samples appear to humans to be obviously altered.

Setup To show this empirically, we increase the ϵ value for a traditional perturbation based attack (a 100-step PGD) until the attack success rates on the certified defenses are similar to those for our technique. Specifically, we used an ϵ of 0.31 and 0.2 to attack [16] and [17] respectively, resulting in success rates of 86.0% and 83.5%. We then asked human annotators to distinguish between the adversarial examples and unmodified images from the dataset, in an A/B test setting. If the two are indistinguishable we expect a 50% success rate.

Results We found that with the perturbation-based examples attacking [16], annotators can correctly identify the adversarial images with a 92.9% success rate, but can only correctly identify adversarial examples from our attack with a 76.8% success rate. Against [17], the success rates are 87.6% and 78.2% respectively. It's important to note that we expect this gap to increase as both better generative models, and better defenses are developed, such that we may expect generative adversarial examples to eventually completely dominate the perturbation-based attacks in evading human detection.

4.3 Targeted attacks against adversarial training

The theoretical guarantees provided by certified defenses are satisfying, however, these defenses require computationally expensive optimization techniques, and so do not yet scale to larger datasets. Furthermore, more traditional defense techniques actually perform better in practice in certain cases. [31] has shown that the strongest non-certified defense currently available is the adversarial training technique presented in [10], so we also evaluated our attack against this defense technique. We perform this evaluation in the targeted setting in order to better understand how the success rate varies between various source target pairs.

Setup We produce 100 generative adversarial examples for each pair of source and target class and ask human annotators to label them. We also compare to traditional PGD attacks as a reference. For the perturbation-based attacks against the ResNet networks, we use a 20-step PGD with the ϵ (out of 1) given in the table. For the perturbation-based attack against the Madry network [10], we simply republish the best public result [36]. It's important to note that the reference perturbation-based results are not directly comparable to the results for our attacks because they are i) untargeted attacks and ii) limited to small perturbations. Nonetheless, they can provide a good sense of the robustness of our adversarially-trained networks.

Results A summary of the results can be seen in Tab. 2. We can see that the [10] defense is quite effective against the basic perturbation-based attack, limiting the success rate to 10.4% on

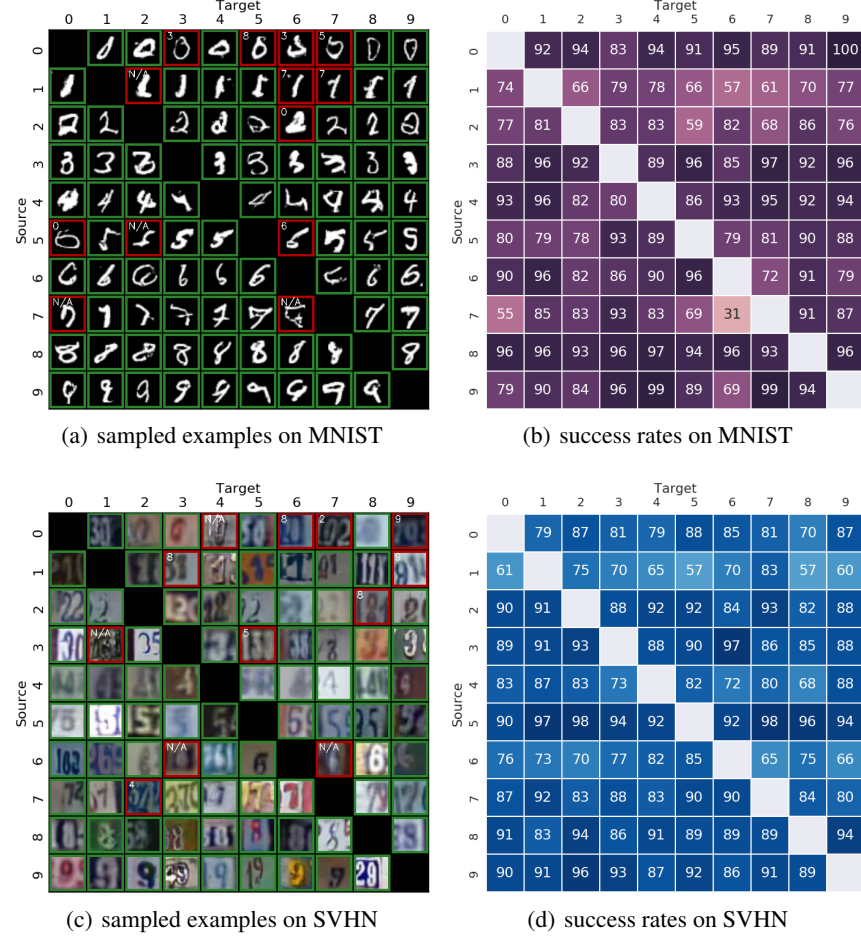


Figure 3: (a)(c) Random samples of targeted generative adversarial examples (w/o noise). Row i and column j is an image that is supposed to be class i and classifier predicts it to be class j . Green border indicates that the image is voted legitimate by MTurk workers, and red border means the label given by workers (as shown in the upper left corner) disagrees with the image’s source class. (b)(d) The success rates (%) of our targeted generative adversarial attack (w/o noise). Also see Tab. 2.

MNIST, and 20.5% on CelebA. However, our generative adversarial examples (with or without noise-augmentation) can successfully fool this defense with more than an 84% success rate on all datasets. We find that adding noise-augmentation to our attack does not significantly change the results, boosting the SVNH success rate by 7.4% while reducing the CelebA success rate by 4.4%. In Fig. 3 and Fig. 4, we show samples and detailed success rates of generative adversarial attacks without noise-augmentation. More samples and success rate details are provide in Appendix D.

4.4 Transferability

An important feature of traditional perturbation-based attacks is their transferability across different classifiers.

Setup To test how our generative adversarial examples transfer to other architectures, we collect all the examples targeting Madry Network [37] on MNIST in Section 4.3, and filter out invalid ones using the majority vote of a set of human annotators. We then feed these generative adversarial examples to other architectures. Besides adversarially-trained Madry Network, the architectures we consider include a ResNet [35] similar to those used on SVHN and CelebA datasets in Section 4.3. We test both normally-trained and adversarially-trained ResNet. We also take the architecture of Madry Network in [10] and train it without adversarial training.

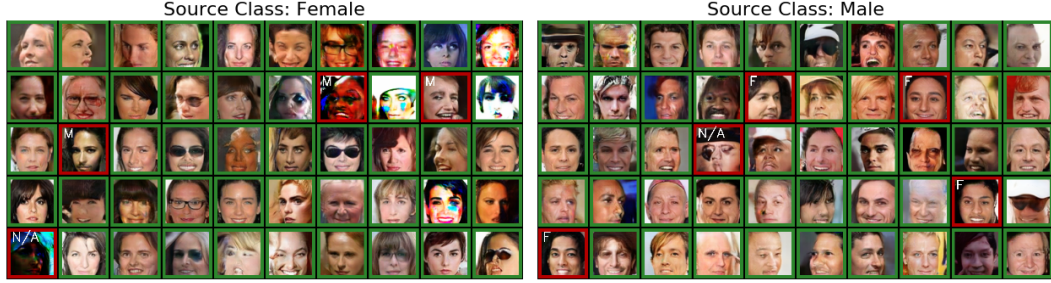


Figure 4: Sampled generative adversarial examples (w/o noise) for fooling the classifier to misclassify a female as male (left) and the other way around (right). Green, red borders and annotations have the same meanings as in Fig. 3, except “F” is short for “Female” and “M” is short for “Male”.

Table 3: Transferability of generative adversarial examples on MNIST. We attack Madry Net [10] (adv) with our method and feed legitimate generative adversarial examples, as verified by AMT workers, to other classifiers. Here “adv” is short for “adversarially-trained” (with PGD) and “no adv” means no adversarial training is used. Numbers represent accuracies of classifiers.

Attack Type \ Classifier	Madry Net [10] (no adv)	Madry Net [10] (adv)	ResNet (no adv)	ResNet (adv)	[16]	[17]
No attack	99.5	98.4	99.3	99.4	95.8	98.2
Our attack (w/o noise)	95.1	0	92.7	93.7	77.1	84.3
Our attack (w/ noise, $\epsilon_{\text{attack}} = 0.3$)	78.3	0	73.8	84.9	78.1	63.0

Results We show in Tab. 3 that generative adversarial examples exhibit moderate transferability to different classifiers, which means they can be threatening in a black-box scenario as well. For attacks without noise-augmentation, the most successful transfer happens against [16], where the success rate is 22.9%. For the noise-augmented attack, the most successful transfer is against [17], with a success rate of 37.0%. The results indicate that the transferability of generative adversarial examples can be generally enhanced with noise-augmentation.

5 Analysis

In this section, we briefly analyze why our method can attack a classifier with generative models, under some necessarily idealized assumptions. For simplicity, we assume the targeted classifier $f(x)$ is binary, where $x \in \mathbb{R}^n$ is the input vector. Previous explanations for perturbation-based attacks [2] assume that the score function $s(x) \in \mathbb{R}$ used by f is almost linear. Suppose $s(x) \approx w^\top x + b$ and $w, x \in \mathbb{R}^n$ both have high dimensions (large n). We can choose the perturbation to be $\delta = \epsilon \text{sign}(w)$, so that $s(x + \delta) - s(x) \approx \epsilon \cdot n$. Though ϵ is small, n is typically a large number, therefore $\epsilon \cdot n$ can be large enough to change the prediction of $f(x)$. Similarly, we can explain the existence of generative adversarial examples. Suppose $g(z, y) \in \mathbb{R}^n$ is an ideal generative model that can always produce legitimate images of class $y \in \{0, 1\}$ for any $z \in \mathbb{R}^m$, and assume for all z^0 , $f(g(z^0, y)) = y$. The end-to-end score function $s(g(z, y))$ can be similarly approximated by $s(g(z, y)) \approx w_g^\top z + b_g$, and we can again take $\delta_z = \epsilon \text{sign}(w_g)$, so that $s(g(z^0 + \delta_z, y)) - s(g(z^0, y)) \approx \epsilon \cdot m$. Because $m \gg 1$ and we can use relatively bigger ϵ in practice, $\epsilon \cdot m$ can be large enough to change the prediction of f , which justifies why we can find many generative adversarial examples by minimizing \mathcal{L} .

It becomes much harder to analyze when our generative model is imperfect, however. We provide an attempt in Appendix A, with some relatively strong assumptions.

6 Conclusion

In this paper, we explore a more general form of adversarial attacks. Instead of perturbing existing data points, our generative adversarial examples are synthesized entirely from scratch, using conditional generative models. As shown in experiments, this new kind of adversarial examples undermines

current defenses, which are designed solely for perturbation-based attacks. Moreover, generative adversarial examples are able to transfer to other classifiers trained using the same dataset, and can be better at evading human detection.

Both traditional perturbation-based attack and the new method proposed in this paper exploit current classifiers' vulnerability to covariate shift [38]. The prevalent training framework in machine learning, Empirical Risk Minimization [39], does not guarantee performance when tested on a different data distribution. Therefore, it is important to develop new training methods that can generalize to different input distributions, or new methods that can reliably detect covariate shift. Such new methods should be able to alleviate threats of both perturbation-based and generative adversarial examples.

Acknowledgements

This research was supported by Intel Corporation, TRI, NSF (#1651565, #1522054, #1733686) and FLI (#2017-158687).

References

- [1] Christian Szegedy, Wojciech Zaremba, Ilya Sutskever, Joan Bruna, Dumitru Erhan, Ian Goodfellow, and Rob Fergus. Intriguing properties of neural networks. *arXiv preprint arXiv:1312.6199*, 2013.
- [2] Ian J Goodfellow, Jonathon Shlens, and Christian Szegedy. Explaining and harnessing adversarial examples. *arXiv preprint arXiv:1412.6572*, 2014.
- [3] Alexey Kurakin, Ian Goodfellow, and Samy Bengio. Adversarial examples in the physical world. *arXiv preprint arXiv:1607.02533*, 2016.
- [4] Kevin Eykholt, Ivan Evtimov, Earlence Fernandes, Bo Li, Amir Rahmati, Chaowei Xiao, Atul Prakash, Tadayoshi Kohno, and Dawn Song. Robust Physical-World Attacks on Deep Learning Visual Classification. In *Computer Vision and Pattern Recognition (CVPR)*, 2018.
- [5] Cihang Xie, Jianyu Wang, Zhishuai Zhang, Yuyin Zhou, Lingxi Xie, and Alan Yuille. Adversarial examples for semantic segmentation and object detection. In *International Conference on Computer Vision. IEEE*, 2017.
- [6] Nicholas Carlini, Pratyush Mishra, Tavish Vaidya, Yuankai Zhang, Micah Sherr, Clay Shields, David Wagner, and Wenchao Zhou. Hidden voice commands. In *USENIX Security Symposium*, pages 513–530, 2016.
- [7] Guoming Zhang, Chen Yan, Xiaoyu Ji, Tianchen Zhang, Taimin Zhang, and Wenyuan Xu. Dolphnattack: Inaudible voice commands. In *Proceedings of the 2017 ACM SIGSAC Conference on Computer and Communications Security*, pages 103–117. ACM, 2017.
- [8] Moustapha Cisse, Yossi Adi, Natalia Neverova, and Joseph Keshet. Houdini: Fooling deep structured prediction models. *arXiv preprint arXiv:1707.05373*, 2017.
- [9] Alexey Kurakin, Ian Goodfellow, and Samy Bengio. Adversarial machine learning at scale. *arXiv preprint arXiv:1611.01236*, 2016.
- [10] Aleksander Madry, Aleksandar Makelov, Ludwig Schmidt, Dimitris Tsipras, and Adrian Vladu. Towards deep learning models resistant to adversarial attacks. *arXiv preprint arXiv:1706.06083*, 2017.
- [11] Aman Sinha, Hongseok Namkoong, and John Duchi. Certifiable distributional robustness with principled adversarial training. *arXiv preprint arXiv:1710.10571*, 2017.
- [12] Shixiang Gu and Luca Rigazio. Towards deep neural network architectures robust to adversarial examples. *arXiv preprint arXiv:1412.5068*, 2014.
- [13] Yang Song, Taesup Kim, Sebastian Nowozin, Stefano Ermon, and Nate Kushman. Pixeldefend: Leveraging generative models to understand and defend against adversarial examples. In *International Conference on Learning Representations*, 2018.
- [14] Pouya Samangouei, Maya Kabkab, and Rama Chellappa. Defense-gan: Protecting classifiers against adversarial attacks using generative models. 2018.

[15] Moustapha Cisse, Piotr Bojanowski, Edouard Grave, Yann Dauphin, and Nicolas Usunier. Parseval networks: Improving robustness to adversarial examples. In *International Conference on Machine Learning*, pages 854–863, 2017.

[16] Aditi Raghunathan, Jacob Steinhardt, and Percy Liang. Certified defenses against adversarial examples. In *International Conference on Learning Representations*, 2018.

[17] J Zico Kolter and Eric Wong. Provable defenses against adversarial examples via the convex outer adversarial polytope. *arXiv preprint arXiv:1711.00851*, 2017.

[18] Tom B Brown, Dandelion Mané, Aurko Roy, Martín Abadi, and Justin Gilmer. Adversarial patch. *arXiv preprint arXiv:1712.09665*, 2017.

[19] Ian Goodfellow, Jean Pouget-Abadie, Mehdi Mirza, Bing Xu, David Warde-Farley, Sherjil Ozair, Aaron Courville, and Yoshua Bengio. Generative adversarial nets. In *Advances in neural information processing systems*, pages 2672–2680, 2014.

[20] Augustus Odena, Christopher Olah, and Jonathon Shlens. Conditional image synthesis with auxiliary classifier gans. In *International Conference on Machine Learning*, pages 2642–2651, 2017.

[21] Ishaan Gulrajani, Faruk Ahmed, Martin Arjovsky, Vincent Dumoulin, and Aaron C Courville. Improved training of wasserstein gans. In *Advances in Neural Information Processing Systems*, pages 5769–5779, 2017.

[22] Michael Buhrmester, Tracy Kwang, and Samuel D Gosling. Amazon’s mechanical turk: A new source of inexpensive, yet high-quality, data? *Perspectives on psychological science*, 6(1):3–5, 2011.

[23] Yann LeCun, Bernhard Boser, John S Denker, Donnie Henderson, Richard E Howard, Wayne Hubbard, and Lawrence D Jackel. Backpropagation applied to handwritten zip code recognition. *Neural computation*, 1(4):541–551, 1989.

[24] Yuval Netzer, Tao Wang, Adam Coates, Alessandro Bissacco, Bo Wu, and Andrew Y Ng. Reading digits in natural images with unsupervised feature learning. In *NIPS workshop on deep learning and unsupervised feature learning*, volume 2011, page 5, 2011.

[25] Ziwei Liu, Ping Luo, Xiaogang Wang, and Xiaoou Tang. Deep learning face attributes in the wild. In *Proceedings of International Conference on Computer Vision (ICCV)*, 2015.

[26] Jorge Nocedal. Updating quasi-newton matrices with limited storage. *Mathematics of computation*, 35(151):773–782, 1980.

[27] Seyed Mohsen Moosavi Dezfooli, Alhussein Fawzi, and Pascal Frossard. Deepfool: a simple and accurate method to fool deep neural networks. In *Proceedings of 2016 IEEE Conference on Computer Vision and Pattern Recognition (CVPR)*, number EPFL-CONF-218057, 2016.

[28] Nicolas Papernot, Patrick McDaniel, Somesh Jha, Matt Fredrikson, Z Berkay Celik, and Ananthram Swami. The limitations of deep learning in adversarial settings. In *Security and Privacy (EuroS&P), 2016 IEEE European Symposium on*, pages 372–387. IEEE, 2016.

[29] Nicholas Carlini and David Wagner. Towards evaluating the robustness of neural networks. In *Security and Privacy (SP), 2017 IEEE Symposium on*, pages 39–57. IEEE, 2017.

[30] Yanpei Liu, Xinyun Chen, Chang Liu, and Dawn Song. Delving into transferable adversarial examples and black-box attacks. In *International Conference on Learning Representations*, 2017.

[31] Anish Athalye, Nicholas Carlini, and David Wagner. Obfuscated gradients give a false sense of security: Circumventing defenses to adversarial examples. *arXiv preprint arXiv:1802.00420*, 2018.

[32] Martin Arjovsky, Soumith Chintala, and Léon Bottou. Wasserstein gan. *arXiv preprint arXiv:1701.07875*, 2017.

[33] Han Xiao, Kashif Rasul, and Roland Vollgraf. Fashion-mnist: a novel image dataset for benchmarking machine learning algorithms. *arXiv preprint arXiv:1708.07747*, 2017.

[34] Alex Krizhevsky. Learning multiple layers of features from tiny images. 2009.

[35] Kaiming He, Xiangyu Zhang, Shaoqing Ren, and Jian Sun. Deep residual learning for image recognition. In *Proceedings of the IEEE conference on computer vision and pattern recognition*, pages 770–778, 2016.

- [36] Aleksander Madry, Aleksandar Makelov, Ludwig Schmidt, Dimitris Tsipras, and Adrian Vladu. Mnist adversarial examples challenge, 2017.
- [37] Laurens van der Maaten and Geoffrey Hinton. Visualizing data using t-sne. *Journal of machine learning research*, 9(Nov):2579–2605, 2008.
- [38] Hidetoshi Shimodaira. Improving predictive inference under covariate shift by weighting the log-likelihood function. *Journal of statistical planning and inference*, 90(2):227–244, 2000.
- [39] Vladimir Vapnik. *The nature of statistical learning theory*. Springer science & business media, 2013.
- [40] Terence Tao. *Topics in random matrix theory*, volume 132. American Mathematical Soc., 2012.
- [41] Phillippe Rigollet. High-dimensional statistics. *Lecture notes for course 18S997*, 2015.
- [42] Jiří Rohn. Computing the norm $\|a\|_\infty$, 1 is np-hard. *Linear and Multilinear Algebra*, 47(3):195–204, 2000.

A Analysis of imperfect generators

In this section, we give one possible explanation for why in practice generative models can create adversarial examples that fool classifiers. We will now assume that generators not always generate legitimate images from the desired class. We will argue that, under some strong assumptions, when the classifier's prediction contradicts the generator's label conditioning, it is more likely for the classifier to make a mistake, rather than the generator generates an incorrect image.

In order to make our argument, we first need Proposition 1:

Proposition 1. *Let $\mathbf{W} \in \mathbb{R}^{n \times m}$ be a random variable. Assume each entry of \mathbf{W} is bounded, i.e., $|w_{ij}| \leq K$ for all i and j . Furthermore, we assume w_{ij} are jointly independent, and $\mathbb{E}[w_{ij}] \leq \tau$. Then, with probability $1 - \delta$, the following bound holds*

$$\frac{1}{n} \max_{\|\Delta \mathbf{x}\|_\infty \leq \epsilon} \|\mathbf{W} \cdot \Delta \mathbf{x}\|_1 \leq 4\epsilon K \sqrt{\frac{m(m \log 2 + \log \frac{1}{\delta})}{n}} + \epsilon \tau m. \quad (4)$$

Proof. Let $\mathbf{W} = (\mathbf{w}_1^\top, \mathbf{w}_2^\top, \dots, \mathbf{w}_n^\top)^\top$, where \mathbf{w}_i represents the i -th row vector of \mathbf{W} . In order to bound $\max_{\|\Delta \mathbf{x}\|_\infty \leq \epsilon} \|\mathbf{W} \Delta \mathbf{x}\|_1$, we first bound $\|\mathbf{W} \Delta \mathbf{x}\|_1$ for any fixed vector $\Delta \mathbf{x}$ from the ball $\mathcal{B}_\epsilon := \{\mathbf{x} \mid \|\mathbf{x}\|_\infty \leq \epsilon\}$ and then apply union bound. Note that $\|\mathbf{W} \Delta \mathbf{x}\|_1$ can be written as the sum of n terms, i.e., $\|\mathbf{W} \Delta \mathbf{x}\|_1 = |\sum_{i=1}^n \mathbf{w}_i^\top \Delta \mathbf{x}|$, where each term $\mathbf{w}_i^\top \Delta \mathbf{x}$ can be bounded using McDiarmid's inequality [40]

$$\mathbb{P} \left(\sum_{j=1}^m w_{ij}(\Delta x)_j - M_i \geq \lambda \right) \leq \exp \left(\frac{-\lambda^2}{2mK^2\epsilon^2} \right), \quad (5)$$

where $M_i = \sum_{j=1}^m \mathbb{E}[w_{ij}(\Delta x)_j] \leq \epsilon \tau m$, according to the theorem's assumption.

From (5) we conclude the random variable $\mathbf{w}_i^\top \Delta \mathbf{x} - M_i$ is sub-Gaussian [41], hence

$$\begin{aligned} \mathbb{E} [\exp(s|\mathbf{w}_i^\top \Delta \mathbf{x} - M_i|)] &\leq \exp(4s^2 m K^2 \epsilon^2) \\ \Rightarrow \mathbb{E} \left[\exp \left(s \sum_{i=1}^n |\mathbf{w}_i^\top \Delta \mathbf{x} - M_i| \right) \right] &\leq \exp(4s^2 n m K^2 \epsilon^2). \end{aligned}$$

With Markov inequality [40], we obtain

$$\mathbb{P} \left(\sum_{i=1}^n |\mathbf{w}_i^\top \Delta \mathbf{x} - M_i| \geq \lambda \right) \leq \exp(4s^2 n m K^2 \epsilon^2 - s\lambda). \quad (6)$$

Because (6) holds for every $s \in \mathbb{R}$, we can optimize s to get the tightest bound

$$\begin{aligned} \mathbb{P} \left(\sum_{i=1}^n |\mathbf{w}_i^\top \Delta \mathbf{x} - M_i| \geq \lambda \right) &\leq \exp \left(-\frac{\lambda^2}{16nmK^2\epsilon^2} \right) \\ \Rightarrow \mathbb{P} \left(\|\mathbf{W} \Delta \mathbf{x}\|_1 \geq \lambda + \sum_{i=1}^n |M_i| \right) &\leq \exp \left(-\frac{\lambda^2}{16nmK^2\epsilon^2} \right) \\ \Rightarrow \mathbb{P} (\|\mathbf{W} \Delta \mathbf{x}\|_1 \geq \lambda + \tau \epsilon n m) &\leq \exp \left(-\frac{\lambda^2}{16nmK^2\epsilon^2} \right). \end{aligned}$$

Now we are ready to apply union bound to control $\max_{\Delta \mathbf{x} \in \mathcal{B}_\epsilon} \|\mathbf{W} \Delta \mathbf{x}\|_1$. Although \mathcal{B}_ϵ is an infinite set, we only need to consider a finite set of vertices $\mathcal{V}_\epsilon := \{\mathbf{x} \mid x_i \in \{-\epsilon, \epsilon\}, \forall i = 1, 2, \dots, m\}$. To see this, assume $\mathbf{x}^* = \arg \max_{\mathbf{x} \in \mathcal{S}_\epsilon} \|\mathbf{W} \mathbf{x}\|_1$ but $\mathbf{x}^* \notin \mathcal{V}_\epsilon$. Because \mathcal{B}_ϵ is a convex polytope with vertices \mathcal{V}_ϵ , we have $\mathbf{x}^* = \sum_{i=1}^{2^m} \lambda_i \mathbf{v}_i$, where $\lambda_i \in [0, 1]$, $\sum_{i=1}^{2^m} \lambda_i = 1$ and \mathbf{v}_i denotes the i -th vertex

in \mathcal{V}_ϵ . By triangle inequality we have

$$\begin{aligned}
\|\mathbf{W}\mathbf{x}^*\|_1 &= \left\| \sum_{i=1}^{2^m} \lambda_i \mathbf{W}\mathbf{v}_i \right\|_1 \\
&\leq \sum_{i=1}^{2^m} \lambda_i \|\mathbf{W}\mathbf{v}_i\|_1 \\
&\leq \left(\sum_{i=1}^{2^m} \lambda_i \right) \max_{i \in [0, 2^m]} \|\mathbf{W}\mathbf{v}_i\|_1 \\
&= \max_{i \in [0, 2^m]} \|\mathbf{W}\mathbf{v}_i\|_1 \leq \|\mathbf{W}\mathbf{x}^*\|_1.
\end{aligned}$$

Let $\mathbf{v}^* := \arg \max_{\mathbf{v}_i, i \in [0, 2^m]} \|\mathbf{W}\mathbf{v}_i\|_1$. From the above derivation we conclude $\|\mathbf{W}\mathbf{v}^*\|_1 = \|\mathbf{W}\mathbf{x}^*\|_1$ and therefore it is sufficient to only consider \mathcal{V}_ϵ for union bound:

$$\begin{aligned}
\mathbb{P} \left(\max_{\Delta\mathbf{x} \in \mathcal{S}_\epsilon} \|\mathbf{W}\Delta\mathbf{x}\|_1 \geq \lambda + \epsilon\tau nm \right) &= \mathbb{P} \left(\max_{\Delta\mathbf{x} \in \mathcal{V}_\epsilon} \|\mathbf{W}\Delta\mathbf{x}\|_1 \geq \lambda + \epsilon\tau nm \right) \\
&\leq |\mathcal{V}_\epsilon| \mathbb{P} (\|\mathbf{W}\Delta\mathbf{x}\|_1 \geq \lambda + \epsilon\tau nm) \quad (\text{Union Bound}) \\
&\leq 2^m \exp \left(-\frac{\lambda^2}{16nmK^2\epsilon^2} \right).
\end{aligned}$$

In other words, with probability $1 - \delta$,

$$\max_{\Delta\mathbf{x} \in \mathcal{S}_\epsilon} \|\mathbf{W}\Delta\mathbf{x}\|_1 \leq 4K\epsilon \sqrt{mn \left(m \log 2 + \log \frac{1}{\delta} \right)} + \epsilon\tau nm,$$

and the statement of our theorem gets proved. \square

Now we show how to apply Proposition 1 to our problem.

Notations Let $s(x)$ be the score function of interest, where $x \in \mathbb{R}^n$ is an input image. Let the targeted classifier be $f(x) = \text{sign}(s(x))$. Given a latent code $z \in \mathbb{R}^m$ and a conditioning label $y \in \{-1, 1\}$, our generative model g produces an image $g(z, y) \in \mathbb{R}^n$. We denote the prior distribution of z as P_z . Additionally, let $\mathbf{J}_{g(z_0, y_0)} \in \mathbb{R}^{n \times m}$ be the Jacobian of $g(z, y)$ w.r.t. z , when $z = z_0$ and $y = y_0$. We similarly define $\mathbf{J}_{s(g(z_0, y_0))} \in \mathbb{R}^{1 \times m}$ to be the Jacobian of $s(g(z, y))$. When $z_0 \sim P_z$ and y_0 is fixed, $\mathbf{J}_{g(z_0, y_0)}$ and $\mathbf{J}_{s(g(z_0, y_0))}$ become random matrices, which we denote as $\mathbf{J}_g \in \mathbb{R}^{n \times m}$ and $\mathbf{J}_s \in \mathbb{R}^{1 \times m}$ respectively. Finally, let J_{ij}^g and J_{ij}^s be the i -th row and j -th column entry of \mathbf{J}_g and \mathbf{J}_s .

Assumptions We make the following assumptions.

1. $\{J_{ij}^g \mid 1 \leq i \leq n, 1 \leq j \leq m\}$ and $\{J_{ij}^s \mid i = 1, 1 \leq j \leq m\}$ are both mutual independent.
2. $\max_{1 \leq i \leq n, 1 \leq j \leq m} |J_{ij}^g| \leq K$ and $\max_{i=1, 1 \leq j \leq m} |J_{ij}^s| \leq K$.
3. $\max_{1 \leq i \leq n, 1 \leq j \leq m} |\mathbb{E}[J_{ij}^g]| \leq \tau$ and $\max_{i=1, 1 \leq j \leq m} |\mathbb{E}[J_{ij}^s]| \leq \tau$.
4. $\tau \ll K$.
5. The gap between L.H.S. and R.H.S. of (4) in Proposition 1 is the same.
6. $o(x) = o(x')$ if $\|x - x'\|_1$ is small.

Conclusion With high probability, when sampling $z^0 \sim P_z$ randomly, we have

$$\max_{\|\delta_z\|_\infty \leq \epsilon} \frac{1}{n} \|g(z^0 + \delta_z, y) - g(z^0, y)\|_1 \ll \max_{\|\delta_z\|_\infty \leq \epsilon} |s(g(z^0 + \delta_z, y)) - s(g(z^0, y))|. \quad (7)$$

Consider our algorithm of creating generative adversarial examples, where we search z within $\|z - z^0\|_\infty \leq \epsilon$ so that $f(g(z, y)) \neq o(g(z, y))$. From (7) we know that the worst perturbation per dimension of $g(z, y)$ is usually much smaller than that of $s(g(z, y))$. If $o(g(z^0, y)) = y$, this means $o(g(z, y)) = y$ is more likely to hold than $o(g(z, y)) = f(g(z, y))$ (according to Assumption 6), which means f is more likely to make the mistake.

Arguments for conclusion Both sides of (7) are hard to quantify in general (actually computing the L.H.S. is NP-hard [42]). We choose to rely on Assumption 5 and propose to compare their upper bounds.

Let $z^0 \sim P_z$ and $\|\delta_z\|_\infty \leq \epsilon$. We can approximate $\|g(z^0 + \delta_z, y) - g(z^0, y)\|_1 \approx \|\mathbf{J}_{g(z^0, y)} \delta_z\|_1$ and $|s(g(z^0 + \delta_z, y)) - s(g(z^0, y))| \approx |\mathbf{J}_{s(g(z^0, y))} \delta_z|$. If all assumptions are true, we can apply Proposition 1 and see that the first term on R.H.S. of (4) dominates the upper bound. Since $\mathbf{J}_g \in \mathbb{R}^{n \times m}$ and $\mathbf{J}_s \in \mathbb{R}^{1 \times m}$, it is clear that the upper bound for $\max_{\|\delta_z\|_\infty \leq \epsilon} \frac{1}{n} \|g(z^0 + \delta_z, y) - g(z^0, y)\|_1$ is much smaller than that of $\max_{\|\delta_z\|_\infty \leq \epsilon} |s(g(z^0 + \delta_z, y)) - s(g(z^0, y))|$, especially when $n \gg 1$. This justifies our conclusion.

B Pseudocode

Algorithm 1 Generative Adversarial Example Targeted Attack

```

1: procedure ATTACK( $y_{\text{target}}$ ,  $y_{\text{source}}$ ,  $f, \theta, \phi, \epsilon, \epsilon_{\text{attack}}, \lambda_1, \lambda_2, \alpha, T$ )
2:   Define  $\mathcal{L}(z, \tau; z^0, y_{\text{target}}, y_{\text{source}}, f, \theta, \phi, \epsilon, \epsilon_{\text{attack}}, \lambda_1, \lambda_2)$ 

$$\mathcal{L} = -\log p(f(g_\theta(z, y_{\text{source}}) + \epsilon_{\text{attack}} \tanh(\tau)) = y_{\text{target}}) + \lambda_1 \cdot \frac{1}{m} \sum_{i=1}^m \max\{|z_i - z_i^0|, \epsilon\}$$


$$- \lambda_2 \cdot \log p(c_\phi(g_\theta(z, y_{\text{source}}) + \epsilon_{\text{attack}} \tanh(\tau)) = y_{\text{source}})$$

3:   Initialize  $x_{\text{attack}} \leftarrow \emptyset$ 
4:   while  $x_{\text{attack}} = \emptyset$  do
5:     Sample  $\tau \sim \mathcal{N}(0, 1)$ 
6:     Sample  $z^0 \sim \mathcal{N}(0, 1)$ 
7:     Initialize  $z \leftarrow z^0$ 
8:     for  $i = 1 \dots T$  do
9:       Update  $z \leftarrow z - \alpha \cdot \frac{\partial \mathcal{L}(z, \tau)}{\partial z}$  ▷  $\alpha$  is the learning rate.
10:       $\Delta \leftarrow \frac{\partial \mathcal{L}(z, \tau)}{\partial \tau}$ 
11:      Update  $\tau \leftarrow \tau - \alpha \cdot \frac{\Delta}{\|\Delta\|}$  ▷ We found gradient normalization to be effective
12:    end for
13:     $x \leftarrow g_\theta(z, y_{\text{source}}) + \epsilon_{\text{attack}} \tanh(\tau)$ 
14:    if  $y_{\text{target}} = \arg \max_y p(f(x) = y)$  then
15:       $x \leftarrow x_{\text{attack}}$ 
16:    end if
17:  end while
18:  return  $x_{\text{attack}}$ 
19: end procedure

```

C Detailed experimental settings

Datasets The datasets used in our experiments are MNIST [23], SVHN [24], and CelebA [25]. Both MNIST and SVHN are images of digits. MNIST contains 60000 28-by-28 gray-scale digits in the training set, and 10000 digits in the test set. In SVHN, there are 73257 32-by-32 images of house numbers (captured from Google Street View) for training, 26032 images for testing, and 531131 additional images as extra training data. For CelebA, there are 202599 celebrity faces, each of which has 40 binary attribute annotations. We group the face images according to female/male, and focus on gender classification. The first 150000 images are split for training and the rest are used for testing.

Adversarial training Regarding adversarial training, we directly use the weights provided by [10] for MNIST. For other tasks, we combine the techniques from [10] and [9]. More specifically, suppose pixel space is $[0, 255]$. We first sample ϵ from $\mathcal{N}(0, 8)$, take the absolute value and truncate it to $[0, 16]$, after which we use PGD with ϵ and iteration number $\lfloor \min(\epsilon + 4, 1.25\epsilon) \rfloor$ to generate adversarial examples for adversarial training. As suggested in [9], this has the benefit of making models robust to attacks with different ϵ .

Table 4: Hyperparameters of generative adversarial attacks. Notations are the same as in Algorithm 1.
 *Target class is “Male”. \dagger Target class is “Female”.

Datasets	Classifier	Targeted	Noise	λ_1	λ_2	ϵ	ϵ_{attack}	α	T
MNIST	Madry Net [10]	Yes	No	50	0	0.1	0	1	500
MNIST	Madry Net [10]	Yes	Yes	50	0	0.1	0.3	1	500
MNIST	[16]	No	No	100	0	0.1	0	10	100
MNIST	[17]	No	No	100	0	0.1	0	1	100
SVHN	ResNet	Yes	No	100	100	0.01	0	0.1	200
SVHN	ResNet	Yes	Yes	100	100	0.01	0.03	0.5	300
CelebA*	ResNet	Yes	No	100	100	0.001	0	1	200
CelebA*	ResNet	Yes	Yes	100	100	0.001	0.03	1	200
CelebA \dagger	ResNet	Yes	No	100	100	0.1	0	0.1	200
CelebA \dagger	ResNet	Yes	Yes	100	100	0.1	0.03	0.1	200

Model architectures For the AC-GAN architecture, we mostly follow the best designs tested in [21]. Specifically, we adapted their AC-GAN architecture on CIFAR-10 for our experiments of MNIST and SVHN, and used their AC-GAN architecture on 64×64 LSUN for our CelebA experiments. Since MNIST digits have lower resolution than CIFAR-10 images, we reduced one residual block in the generator so that the output shape is smaller, and reduced the channels of output from 3 to 1. The other components of AC-GAN, including architecture of the discriminator and auxiliary classifier, are all the same as described in [21].

For classifier architectures, we obtained networks and weights from authors of [10, 16, 17] so that we can be consistent with their papers. The ResNet architectures used for SVHN, CelebA and transferability experiments are shown in Tab. 5.

Hyperparameters of attacks Tab. 4 shows our hyperparameters of all generative adversarial attacks used in this paper, following the same notations in arguments of Algorithm 1.

Table 5: ResNet Classifier Architecture. We set the base number of feature maps to $m = 4$ for MNIST and $m = 16$ for SVHN and CelebA.

Name	Configuration	Replicate Block
Initial Layer	3×3 conv. m maps. 1×1 stride.	—
Residual Block 1	batch normalization, leaky relu 3×3 conv. m maps. 1×1 stride batch normalization, leaky relu 3×3 conv. m maps. 1×1 stride residual addition	$\times 10$
Resize Block 1	batch normalization, leaky relu 3×3 conv. $2m$ maps. 2×2 stride batch normalization, leaky relu 3×3 conv. $2m$ maps. 1×1 stride average pooling, padding	—
Residual Block 2	batch normalization, leaky relu 3×3 conv. $2m$ maps. 1×1 stride batch normalization, leaky relu 3×3 conv. $2m$ maps. 1×1 stride residual addition	$\times 9$
Resize Block 2	batch normalization, leaky relu 3×3 conv. $4m$ maps. 2×2 stride batch normalization, leaky relu 3×3 conv. $4m$ maps. 1×1 stride average pooling, padding	—
Residual Block 3	batch normalization, leaky relu 3×3 conv. $4m$ maps. 1×1 stride batch normalization, leaky relu 3×3 conv. $4m$ maps. 1×1 stride residual addition	$\times 9$
Pooling Layer	batch normalization, leaky relu, average pooling	—
Output Layer	10 dense, softmax	—

D Additional samples

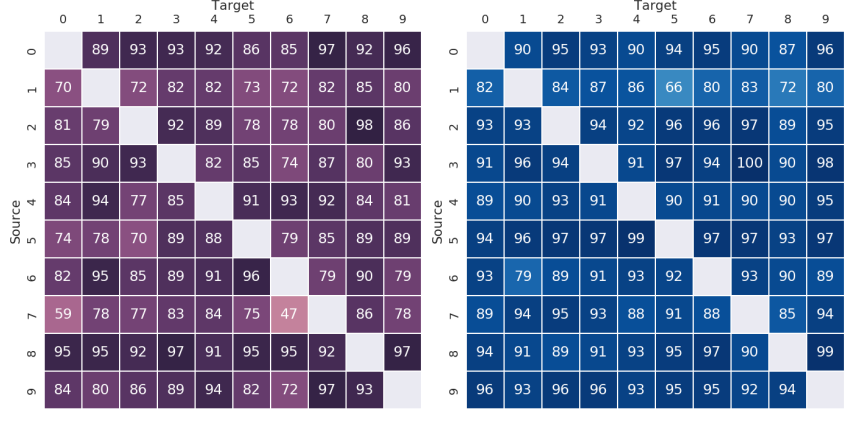


(a) Extended plot for untargeted attacks against [16].



(b) Extended plot for untargeted attacks against [17].

Figure 5: (Extended plot of Fig. 1) Random samples of untargeted generative adversarial examples (w/o noise) against certified defenses on MNIST. Green and red borders indicate success/failure respectively, according to MTurk results. The annotation in upper-left corner of each image represents the classifier's prediction.



(a) success rates on MNIST

(b) success rates on SVHN

Figure 6: The success rates (%) of our targeted generative adversarial attack with noise-augmentation.

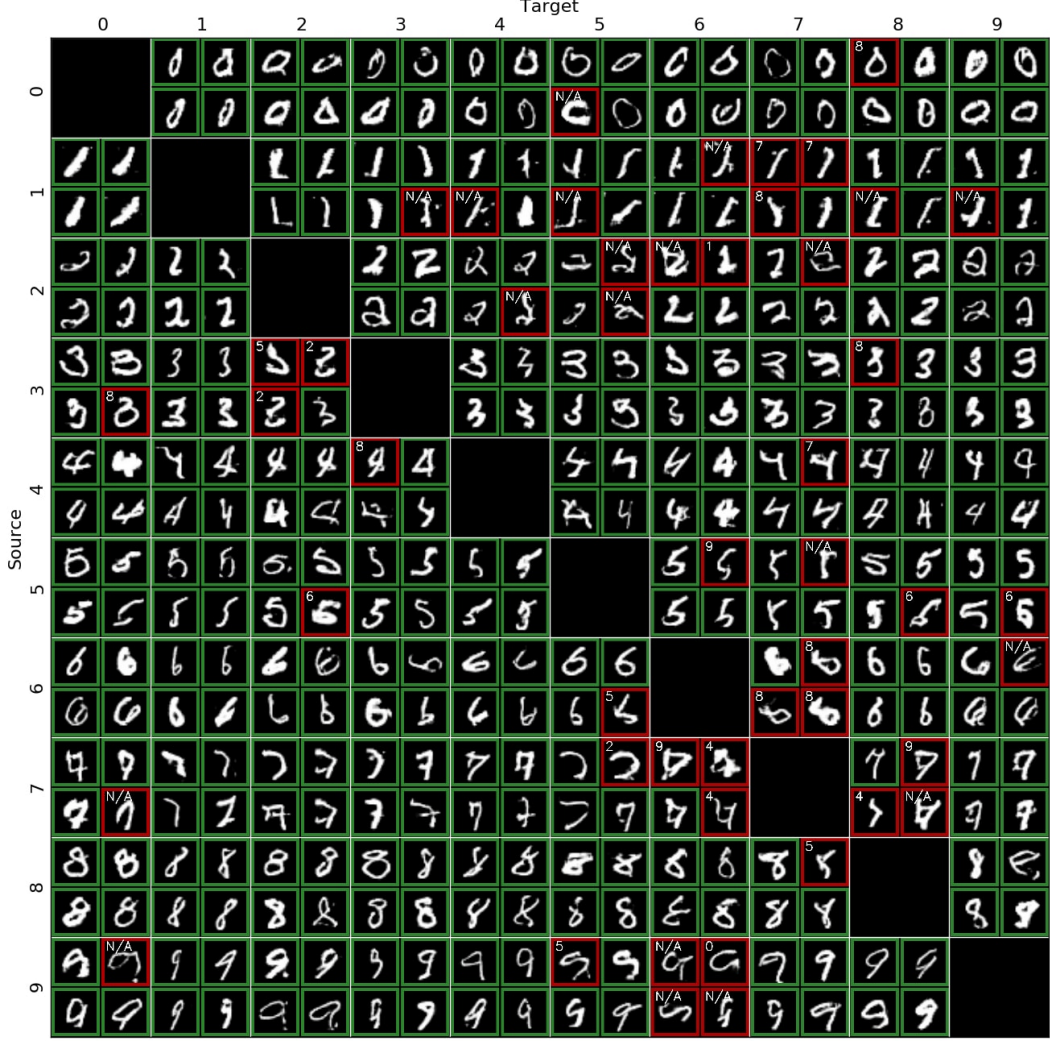


Figure 7: (Extended plot of Fig. 3(a)) Random samples of targeted generative adversarial examples (w/o noise) on MNIST. Green border indicates that the image is voted legitimate by MTurk workers, and red border means the label given by workers (as shown in the upper left corner) disagrees with the image's source class.

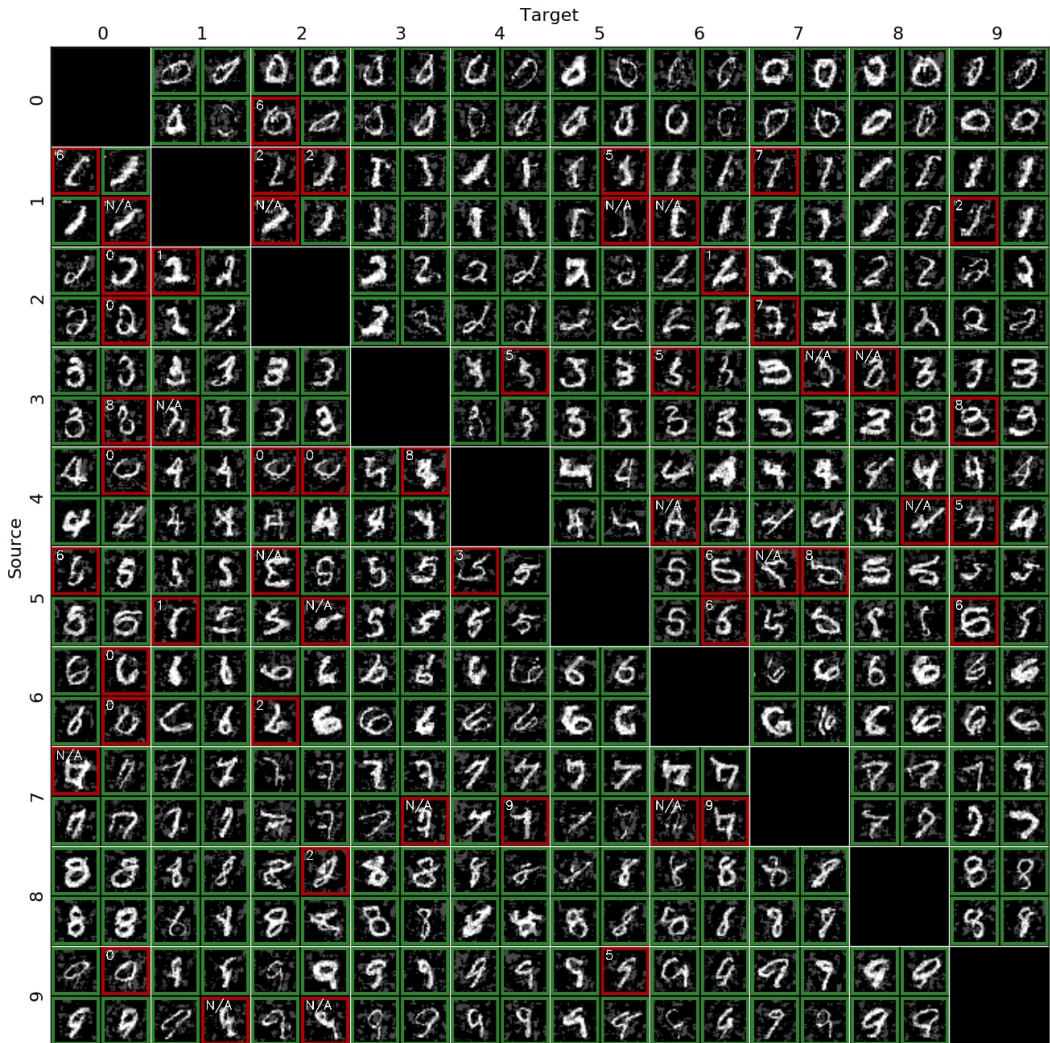


Figure 8: Random samples of targeted generative adversarial examples (w/ noise) on MNIST. Green border indicates that the image is voted legitimate by MTurk workers, and red border means the label given by workers (as shown in the upper left corner) disagrees with the image's source class.



Figure 9: (Extended plot of Fig. 3(c)) Random samples of targeted generative adversarial examples (w/o noise) on SVHN. Green border indicates that the image is voted legitimate by MTurk workers, and red border means the label given by workers (as shown in the upper left corner) disagrees with the image's source class.

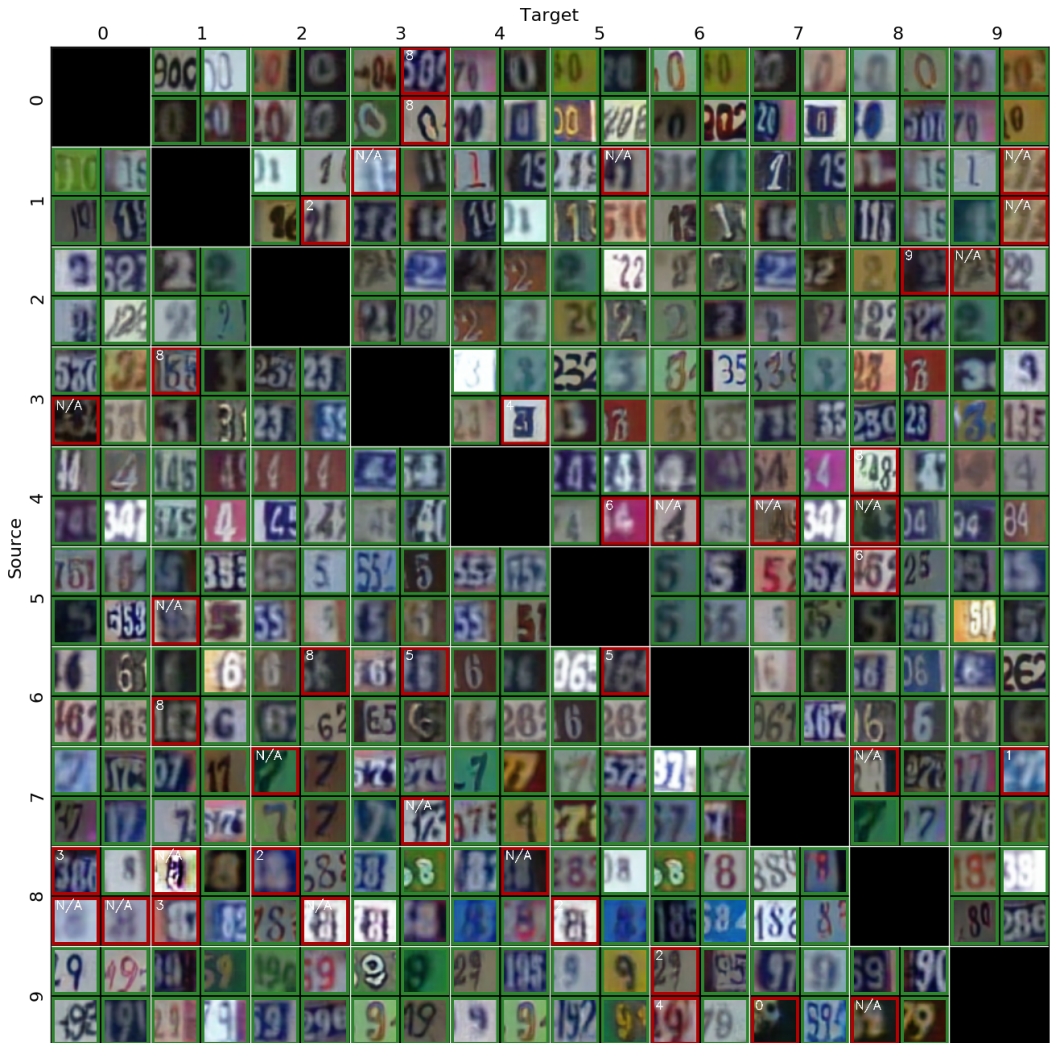


Figure 10: Random samples of targeted generative adversarial examples (w/ noise) on SVHN. Green border indicates that the image is voted legitimate by MTurk workers, and red border means the label given by workers (as shown in the upper left corner) disagrees with the image's source class.

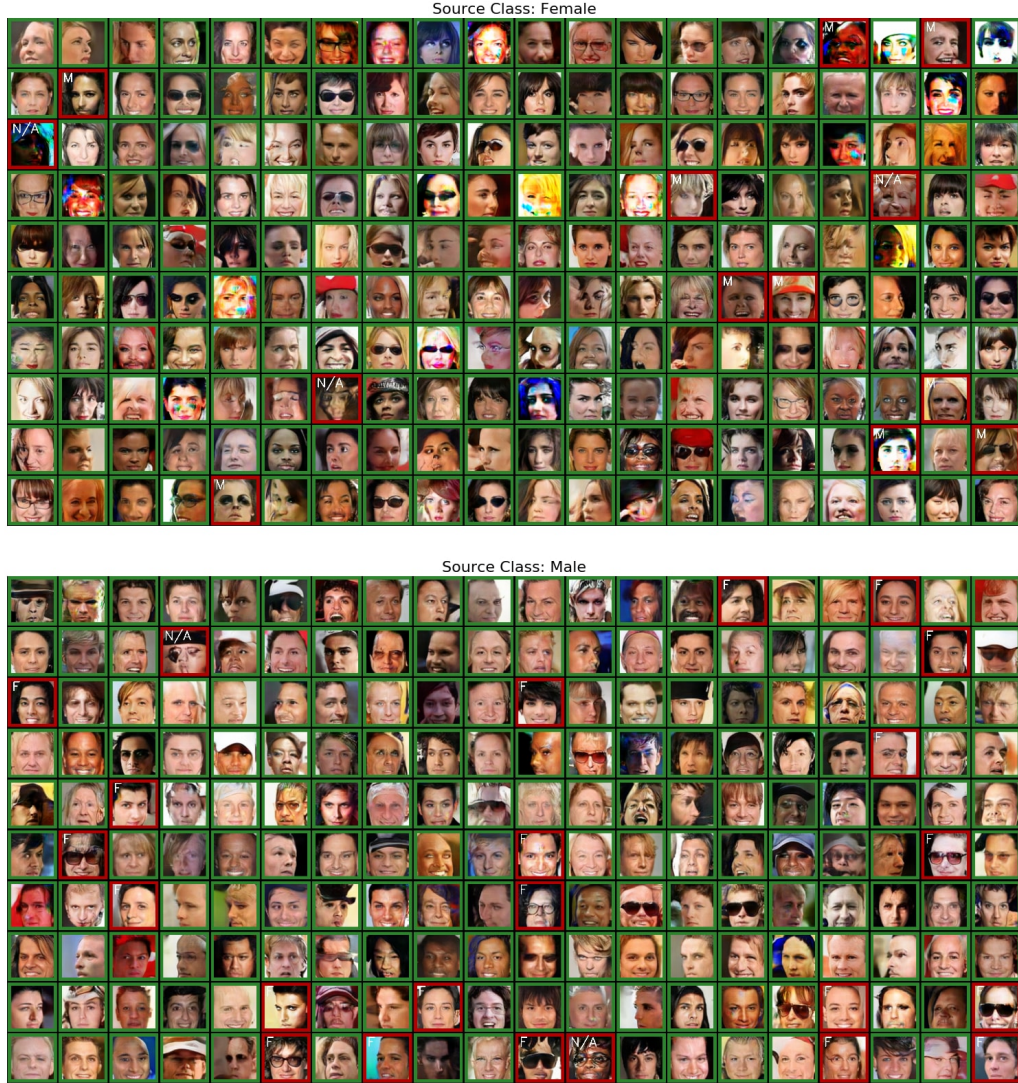


Figure 11: (Extended plot of Fig. 4) Sampled generative adversarial examples (w/o noise) for fooling the classifier to misclassify a female as male (left) and the other way around (right). Green, red borders and annotations have the same meanings as in Fig. 3, except “F” is short for “Female” and “M” is short for “Male”.



Figure 12: Sampled generative adversarial examples (w/ noise) for fooling the classifier to misclassify a female as male (left) and the other way around (right). Green, red borders and annotations have the same meanings as in Fig. 3, except “F” is short for “Female” and “M” is short for “Male”.

E MTurk web interfaces

The MTurk web interfaces used for labeling our generative adversarial examples are depicted in Fig. 13. The A/B test interface used in Section 4.2.1 is shown in Fig. 14. In addition, Fig. 15 visualizes the uncertainty of MTurk annotators for labeling generative adversarial examples, which indicates that more than 40%-50% generative adversarial examples (depending on the dataset) get all of their 5 annotators agreed on one label.

Image Tagging Instructions, please read! (click to collapse)

You must identify the digit shown in the following image

- Select the digit below each image
- If an image contains several digits, tag the digit closer to the **middle** of the image.
- Select N/A only when the image doesn't look close to any digit. It's OK if the digit is blurry, noisy or looks artificial.**
- Irresponsible answers will be **REJECTED** and you **WON'T BE PAID**.
- Examples:

<table border="1"> <tr><td>0</td><td>1</td><td>2</td></tr> <tr><td>3</td><td>4</td><td>5</td></tr> <tr><td>6</td><td>7</td><td>8</td></tr> <tr><td>9</td><td>N/A</td><td></td></tr> </table>	0	1	2	3	4	5	6	7	8	9	N/A		<table border="1"> <tr><td>0</td><td>1</td><td>2</td></tr> <tr><td>3</td><td>4</td><td>5</td></tr> <tr><td>6</td><td>7</td><td>8</td></tr> <tr><td>9</td><td>N/A</td><td></td></tr> </table>	0	1	2	3	4	5	6	7	8	9	N/A	
0	1	2																							
3	4	5																							
6	7	8																							
9	N/A																								
0	1	2																							
3	4	5																							
6	7	8																							
9	N/A																								

Image:

Digit:

0	1	2
3	4	5
6	7	8
9	N/A	

0	1	2
3	4	5
6	7	8
9	N/A	

0	1	2
3	4	5
6	7	8
9	N/A	

0	1	2
3	4	5
6	7	8
9	N/A	

0	1	2
3	4	5
6	7	8
9	N/A	

Image:

Digit:

0	1	2
3	4	5
6	7	8
9	N/A	

0	1	2
3	4	5
6	7	8
9	N/A	

0	1	2
3	4	5
6	7	8
9	N/A	

0	1	2
3	4	5
6	7	8
9	N/A	

0	1	2
3	4	5
6	7	8
9	N/A	

Submit

(a) The MTurk web interface for MNIST and SVHN.

Gender Tagging Instructions, please read! (click to collapse)

You must identify the genders of faces shown in the images

- Select the gender of each human face image.
- Select N/A only when the image contains no human face or the face is heavily distorted**
- Irresponsible answers will be **REJECTED** and you **WON'T GET PAID**.
- Examples:

Female	Female	Female	Female
Male	Male	Male	Male
N/A	N/A	N/A	N/A

Image:

Gender:

Female
Male
N/A

Female
Male
N/A

Female
Male
N/A

Female
Male
N/A

Female
Male
N/A

Image:

Digit:

Female
Male
N/A

Female
Male
N/A

Female
Male
N/A

Female
Male
N/A

Female
Male
N/A

Submit

(b) The MTurk web interface for CelebA.

Figure 13: MTurk web interfaces for labeling generative adversarial examples.

Instructions, please read! (click to collapse)

You must identify which digit is real and which is synthesized by the computer:

- For each group of digits, there is one drawn by human beings (real) and another generated by a computer program (fake).
- Try your best to identify the fake image, i.e., the one generated by the computer.
- Clean your screen and increase its brightness** before working on this HIT! The fake images are usually **noisy/spotty/unnatural** in some way.
- Examples:

<input type="radio"/> Top	<input type="radio"/> Top
<input type="radio"/> Bottom	<input type="radio"/> Bottom

Image (Top):				
Image (Bottom):				
Which is fake:	<input type="radio"/> Top <input type="radio"/> Bottom			
Submit				

Figure 14: MTurk web interfaces for A/B test on MNIST.

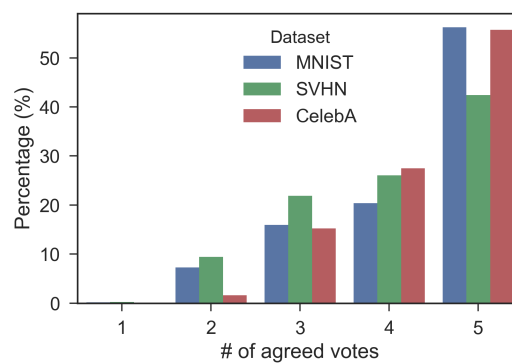


Figure 15: The distribution of number of agreed votes for each image. For example, the red bar on top of 5 means around 55% generative adversarial examples on CelebA dataset are voted the same label by all 5 MTurk annotators.